

专栏:电磁波传输与调控

墙体中金属细导体目标的电磁散射特性研究

李雪萍,李玉莹,张启萌,李玮

(河南师范大学 电子与电气工程学院;河南省电磁波工程院士工作站,河南 新乡 453007)

摘要:建立了建筑物墙体结构探测雷达的物理模型,提出了一种墙体中金属细导体目标散射的偶极子源计算方法,利用分层介质中偶极子公式结合边界条件和矩量法得到了墙体中金属细导体在墙外任一点的散射场强度,并将计算结果与时域有限差分数值模拟结果进行了比较,结果表明该方法能够实现对墙体中金属细导体目标散射场的快速计算和分析,可以为墙体结构探测雷达成像和电磁学反演方法提供一种快速算法。

关键词:分层介质;细导体;散射特性;偶极子源

中图分类号:TN957

文献标志码:A

近年来,诸多工程应用,如地下结构探测、墙体中目标的探测与识别以及地海面雷达目标隐身等,都需要深入开展分层媒质中目标的电磁辐射与散射分析方法的研究.媒质的分层模型是对空间非均匀复杂电磁环境的一种近似模拟,是众多电磁场工程应用实例的数学物理抽象,如何对分层媒质环境下的辐射问题进行精确的数值分析和建模一直是计算电磁学领域的难题^[1-5].

在近距离超宽带雷达探测应用中,除去表层穿透雷达外,另一个比较重要的应用就是建筑物墙体结构探测雷达.此雷达是通过发射电磁波来获取隐藏在墙体中的目标信息.若能正确分析这些信息,将会对目标的成像和识别产生重要作用.近几十年,建筑物墙体结构雷达的探测技术已经广泛应用于生命检测、反恐维稳和灾害救援等方面^[6-10].但实地的测量实验需要消耗大量的人力和物力,这对于研究工作来说是不可取的.而墙体中目标的电磁响应数值分析却可以为超宽带雷达信号的研究和分析提供原始数据,因此本文重点研究墙体中目标对天线的电磁散射特性.

近年来,不同学者对分层介质中圆柱体目标的电磁散射都做了大量研究^[11-16],GAO等^[11]结合实验对有耗半空间中的天线特性作了研究;ZU等^[13]分析了跨半空间界面的二维柱体目标的散射;HU等^[15]则对分层介质上方复杂电大尺寸目标的电磁散射进行了求解计算,除此之外,半空间随机粗糙面的散射特性分析也被研究^[17-19].这些研究中很少涉及分层介质中圆柱导体目标对点源的散射场推导.因为对点源而言,即使导体无限长,散射问题也是一个三维问题,此时给出圆柱体边界上所有点都符合边界条件的解析表达式非常困难.针对这一实际情况结合建筑物墙体结构探测雷达应用场景本文提出一种对细圆柱导体的近似解法,将圆柱边界上所有点需符合边界条件的要求用仅沿导体轴线表面电场为零的边界条件来代替.在这种近似下,三维问题可以演变成二维问题,使原来不能用解析方法分析的问题变成了可解问题.本文首先根据实际工作场景建立了物理模型,利用分层介质中偶极子公式结合边界条件和矩量法对金属细目标体的散射场进行了详细推导,并将计算结果与时域有限差分数值模拟结果进行了比较,结果表明该方法能够实现对墙体中金属细导体目标散射场的计算和分析.

收稿日期:2023-03-06;**修回日期:**2023-05-08.

基金项目:国家自然科学基金(42004064);河南省科技攻关项目(232102210164);河南省高等学校重点科研项目(22B510008);河南师范大学博士科研启动项目(5101239170009).

作者简介(通信作者):李玮(1981—),女,河南洛阳人,河南师范大学副教授,博士,研究方向为天线与电波传播,超材料设计及应用,E-mail:wli829@126.com.

1 物理模型

本文根据超宽带雷达实际应用场景建立了建筑物墙体结构中细导体目标的电磁散射物理模型,如图 1 所示.该模型由 2 层自由空间层(0 区和 2 区)以及中间厚度为 H 的墙体(1 区)组成,相对介电常数分别为 ϵ_0 和 ϵ_1 ;建筑物墙体结构中埋有一细长导体,该导体长度为 l ,半径为 r_a ,距离墙体表面距离为 h_1 .建筑物墙体结构探测雷达向墙体发射电磁波,电磁波在穿透墙体与目标发生作用后被反射回来.这里将天线假设为一具有单位电偶矩的水平电偶极子.在主坐标系(O, X, Z)中,水平电偶极子与建筑物墙体表面的垂直距离为 h_0 ,其偶极矩的方向沿 x ,将长度为 l 的导体等分为 m 段;第 2 个坐标系(O_t, X_t, Z_t)的原点位于导体第 t 段($t=1, 2, \dots, m$)的中心;第 3 个坐标系(K, ξ, ζ)则以墙体表面为原点.

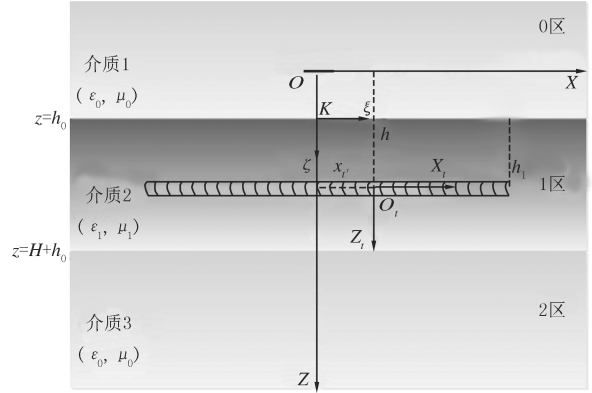


图1 建筑物墙体结构中细导体目标的电磁散射物理模型(OXZ 平面上)
Fig.1 Physical model for electromagnetic scattering of slim metal conductor buried in the wall(OXZ -Plane)

2 散射场的推导

2.1 区域 1 中入射场

波动方程的解可以理解成 TE 波和 TM 波分量的线性叠加.在谱域中,设 A_l 和 B_l 为 TM 波的幅度, C_l 和 D_l 为 TE 波的幅度^[20].对于区域 0 中,其波幅

$$A_{0+} = \frac{1 - R_{0-}^{\text{TM}}}{1 - R_{0+}^{\text{TM}} R_{0-}^{\text{TM}}} E_{\text{hed}}, B_{0+} = \frac{R_{0+}^{\text{TM}} (1 - R_{0-}^{\text{TM}})}{1 - R_{0+}^{\text{TM}} R_{0-}^{\text{TM}}} E_{\text{hed}}, C_{0+} = \frac{1 + R_{0-}^{\text{TE}}}{1 - R_{0+}^{\text{TE}} R_{0-}^{\text{TE}}} H_{\text{hed}}, D_{0+} = \frac{R_{0+}^{\text{TE}} (1 + R_{0-}^{\text{TE}})}{1 - R_{0+}^{\text{TE}} R_{0-}^{\text{TE}}} H_{\text{hed}},$$

其中, $E_{\text{hed}} = i \frac{Ilk_{\rho}^2}{8\pi\omega\epsilon_0}$, $H_{\text{hed}} = i \frac{Ilk_{\rho}^2}{8\pi k_{0z}}$, ϵ_0 为自由空间相对介电常数, ω 为角频率, Il 为偶极矩, R_{0-}^{TM} 、 R_{0-}^{TE} 、 R_{0+}^{TM} 和 R_{0+}^{TE} 分别为介质 2 的厚度在分界面上引起的反射系数(下标 0- 表示沿着 z 轴负方向,0+ 表示沿着 z 轴正方向), $R_{0-}^{\text{TM}} = R_{0-}^{\text{TE}} = 0$, $R_{0+}^{\text{TM}} = \frac{B_{0+}}{A_{0+}} = \frac{R_{01}^{\text{TM}} + R_{12}^{\text{TM}} e^{i2k_{1z}H}}{1 + R_{01}^{\text{TM}} R_{12}^{\text{TM}} e^{i2k_{1z}H}} e^{i2k_{0z}h_0}$, $R_{0+}^{\text{TE}} = \frac{D_{0+}}{C_{0+}} = \frac{R_{01}^{\text{TE}} + R_{12}^{\text{TE}} e^{i2k_{1z}H}}{1 + R_{01}^{\text{TE}} R_{12}^{\text{TE}} e^{i2k_{1z}H}} e^{i2k_{0z}h_0}$, $k_{\rho}^2 + k_{0z}^2 = k_0^2$, $k_0 = \omega \sqrt{\mu_0 \epsilon_0}$.

计算过程中首先需要确定 0 区(偶极子所在的空间)的波幅,其他区域的波幅可以通过传播矩阵确定.在圆柱坐标系下,介质 1 和介质 2 交界处的边界条件要求切向电场分量在所有 ρ 和 ϕ 处连续,考虑到上下两介质交界面上的反射.在区域 1 中,将 A_1 和 B_1 分别用 A_0 和 B_0 表示: $A_1 e^{ik_{1z}d_1} = \frac{1}{2} \left[\frac{\epsilon_0}{\epsilon_1} + \frac{k_{0z}}{k_{1z}} \right] [A_{0+} e^{ik_{0z}d_1} - R_{0,1}^{\text{TM}} B_{0+} e^{-ik_{0z}d_1}]$, $B_1 e^{-ik_{1z}d_1} = \frac{1}{2} \left[\frac{\epsilon_0}{\epsilon_1} + \frac{k_{0z}}{k_{1z}} \right] [-R_{0,1}^{\text{TM}} A_{0+} e^{ik_{0z}d_1} + B_{0+} e^{-ik_{0z}d_1}]$. C_1 和 D_1 也可以分别用 C_0 和 D_0 表示,其结果与上面 2 式呈二元对称性.

柱坐标系下区域 1 中电场表达式如文献[18]所示,其沿 x 方向的电场

$$E_{1x}^i(k_{\rho}, X, 0, Z) = E_{1\rho}(k_{\rho}) \cos \phi - E_{1\phi}(k_{\rho}) \sin \phi = \int_{-\infty}^{\infty} dk_{\rho} \frac{ik_{1z}}{k_{\rho}} (A_1 e^{ik_{1z}z} - B_1 e^{-ik_{1z}z}) H_1^{(1)'}(k_{\rho} |x|) + \int_{-\infty}^{\infty} dk_{\rho} \frac{i\omega\mu_1}{k_{\rho}^2 x} (C_1 e^{ik_{1z}z} + D_1 e^{-ik_{1z}z}) H_1^{(1)}(k_{\rho} |x|),$$

式中, $k_{1\rho}^2 + k_{1z}^2 = k_1^2, k_1 = \omega \sqrt{\mu_1 \epsilon_1}$.

2.2 区域1中位于 $(x_t, 0, h)$ 的电偶极子产生的散射场

区域1中金属细导体在入射场作用下产生感应电流, 电流方向与 x 方向相同, 长度为 Δl 的每段导体, 等价于一段重新辐射的水平偶极子, 其偶极矩 $P_t = I_t \Delta l$, 中心位于 $(x_t, 0, h_1 + h_0)$, 方向沿 x . 在研究导体的辐射时, 辐射源处于1区, 它在1区产生的场对应的波幅分别为 $A_{0+}^s, B_{0+}^s, C_{0+}^s, D_{0+}^s, A_{0-}^s, B_{0-}^s, C_{0-}^s$ 和 D_{0-}^s (下标0-表示沿着 z_t 轴负方向, 0+表示沿着 z_t 轴正方向; 上标s表示介质2中感应电流产生的场). 在第2个坐标系 (O_t, X_t, Z_t) 中, 坐标记为 (x', y', z') , $x' = x - x_t, z' = z - h, h = h_0 + h_1$. 在区域1中, 导体辐射时产生的波幅

$$\begin{aligned} A_{0+}^s &= \frac{1 - R_{0-}^{\text{TM},s}}{1 - R_{0+}^{\text{TM},s} R_{0-}^{\text{TM},s}} E'_{\text{hed}}, B_{0+}^s = \frac{R_{0+}^{\text{TM},s} (1 - R_{0-}^{\text{TM},s})}{1 - R_{0+}^{\text{TM},s} R_{0-}^{\text{TM},s}} E'_{\text{hed}}, \\ C_{0+}^s &= \frac{1 + R_{0-}^{\text{TE},s}}{1 - R_{0+}^{\text{TE},s} R_{0-}^{\text{TE},s}} H'_{\text{hed}}, D_{0+}^s = \frac{R_{0+}^{\text{TE},s} (1 + R_{0-}^{\text{TE},s})}{1 - R_{0+}^{\text{TE},s} R_{0-}^{\text{TE},s}} H'_{\text{hed}}, \\ A_{0-}^s &= -\frac{R_{0-}^{\text{TM},s} (1 - R_{0+}^{\text{TM},s})}{1 - R_{0+}^{\text{TM},s} R_{0-}^{\text{TM},s}} E'_{\text{hed}}, B_{0-}^s = \frac{(1 - R_{0+}^{\text{TM},s})}{1 - R_{0+}^{\text{TM},s} R_{0-}^{\text{TM},s}} E'_{\text{hed}}, \\ C_{0-}^s &= \frac{R_{0-}^{\text{TE},s} (1 + R_{0+}^{\text{TE},s})}{1 - R_{0+}^{\text{TE},s} R_{0-}^{\text{TE},s}} H'_{\text{hed}}, D_{0-}^s = \frac{(1 + R_{0+}^{\text{TE},s})}{1 - R_{0+}^{\text{TE},s} R_{0-}^{\text{TE},s}} H'_{\text{hed}}, \end{aligned}$$

其中 $E'_{\text{hed}} = i \frac{P_t k_\rho^2}{8\pi\omega\epsilon_1}, H'_{\text{hed}} = i \frac{P_t k_\rho^2}{8\pi k_{1z}}$, ϵ_1 为介质2的相对介电常数, $R_{0-}^{\text{TM},s}, R_{0-}^{\text{TE},s}$ 和 $R_{0+}^{\text{TM},s}, R_{0+}^{\text{TE},s}$ 分别为介质2的厚度在分界面上引起的反射系数(下标0-表示沿着 z_t 轴负方向, 0+表示沿着 z_t 轴正方向). 其值分别为:

$$\begin{aligned} R_{0+}^{\text{TM},s} &= \frac{B_{0+}^s}{A_{0+}^s} = \frac{e^{i2k_{1z}(H-h_1)}}{R_{12}^{\text{TM}}} + \frac{[1 - (1/R_{12}^{\text{TM}})^2] e^{i2(k_{1z}+k_{2z})(H-h_1)}}{(1/R_{12}^{\text{TM}}) e^{i2k_{2z}(H-h_1)}}, \\ R_{0+}^{\text{TE},s} &= \frac{D_{0+}^s}{C_{0+}^s} = \frac{e^{i2k_{1z}(H-h_1)}}{R_{12}^{\text{TE}}} + \frac{[1 - (1/R_{12}^{\text{TE}})^2] e^{i2(k_{1z}+k_{2z})(H-h_1)}}{(1/R_{12}^{\text{TE}}) e^{i2k_{2z}(H-h_1)}}, \\ R_{0-}^{\text{TM},s} &= \frac{A_{0-}^s}{B_{0-}^s} = \frac{e^{-i2k_{1z}(-h_1)}}{R_{10}^{\text{TM}}} + \frac{[1 - (1/R_{10}^{\text{TM}})^2] e^{-i2(k_{1z}+k_{0z})(-h_1)}}{(1/R_{10}^{\text{TM}}) e^{-i2k_{0z}(-h_1)}}, \\ R_{0-}^{\text{TE},s} &= \frac{C_{0-}^s}{D_{0-}^s} = \frac{e^{-i2k_{1z}(-h_1)}}{R_{10}^{\text{TE}}} + \frac{[1 - (1/R_{10}^{\text{TE}})^2] e^{-i2(k_{1z}+k_{0z})(-h_1)}}{(1/R_{10}^{\text{TE}}) e^{-i2k_{0z}(-h_1)}}, \end{aligned}$$

则偶极矩 P_t 在区域1中沿 x_t 方向产生的电场 $E_{1x}^s(k_\rho, x', 0, z'; x_t) = E_{1\rho}(k_\rho) \cos \phi - E_{1\phi}(k_\rho) \sin \phi = \int_{-\infty}^{\infty} dk_\rho \frac{ik_{1z}}{k_\rho} (A_0^s(P_t) e^{ik_{1z}z'} - B_0^s(P_t) e^{-ik_{1z}z'}) H_1^{(1)'}(k_\rho | x' |) + \int_{-\infty}^{\infty} dk_\rho \frac{i\omega\mu_1}{k_\rho^2 |x'|} (C_0^s(P_t) e^{ik_{1z}z'} + D_0^s(P_t) e^{-ik_{1z}z'}) H_1^{(1)}(k_\rho | x' |)$.

2.3 边界方程

当介质2中所有场表达式推导出来后, 利用金属细导体目标表面的边界条件进行求解. 在 $x = x_t$ 的导体边界上, $z'_- = -r_a, z'_+ = h - r_a$, 沿 x 方向的入射场

$$\begin{aligned} E_{1x}^i(k_\rho, x_t, h - r_a) &= \int_{-\infty}^{\infty} dk_\rho \frac{ik_{1z}}{k_\rho} (A_1 e^{ik_{1z}(h-r_a)} - B_1 e^{-ik_{1z}(h-r_a)}) H_1^{(1)'}(k_\rho | x_t |) + \\ &\int_{-\infty}^{\infty} dk_\rho \frac{i\omega\mu_1}{k_\rho^2 |x_t|} (C_1 e^{ik_{1z}(h-r_a)} + D_1 e^{-ik_{1z}(h-r_a)}) H_1^{(1)}(k_\rho | x_t |). \end{aligned} \quad (1)$$

位于 x_t 的偶极子在 $x = x_t$ 边界上产生的散射场

$$E_{1x}^s(k_\rho, x_t, 0, -r_a; x_t) = \int_{-\infty}^{\infty} dk_\rho \frac{ik_{1z}}{k_\rho} (A_{0-}^s(P_t) e^{-ik_{1z}r_a} - B_{0-}^s(P_t) e^{ik_{1z}r_a}) H_1^{(1)'}[k_\rho | x_t - x_t |] +$$

$$\int_{-\infty}^{\infty} dk_{\rho} \frac{i\omega\mu_1}{k_{\rho}^2 |x_t - x_{t'}|} (C_{0-}^s(P_{t'})e^{-ik_{1z}r_a} + D_{0-}^s(P_{t'})e^{ik_{1z}r_a})H_1^{(1)}[k_{\rho} | x_t - x_{t'} |], \quad (2)$$

此时,在 $x = x_t, z'_t = -r_a$ 处的金属细导体目标表面的总场

$$E_{1x}^i(k_{\rho}, x_t, h - r_a) + \sum_{t'=1}^m E_{1x}^s(k_{\rho}, x_t, 0, -r_a; x_{t'}) = 0 (t = 1, 2, \dots, m). \quad (3)$$

将式(1)和(2)代入式(3),经过化简后可得到一个关于 $P_{t'}$ 的线性方程组

$$\sum_{t'=1}^m G(x_t, x_{t'}) \cdot P_{t'} = -E_{1x}^i(x_t) (t = 1, 2, \dots, m), \quad (4)$$

其中,

$$\begin{aligned} G(x_t, x_{t'}) = & \int_{-\infty}^{\infty} dk_{\rho} \frac{ik_{1z}}{k_{\rho}} \left[-i \frac{R_{0-}^{\text{TM},s}(1 - R_{0+}^{\text{TM},s})}{1 - R_{0+}^{\text{TM},s}R_{0-}^{\text{TM},s}} \frac{k_{\rho}^2}{8\pi\omega\epsilon_1} e^{-ik_{1z}r_a} + i \frac{(1 - R_{0+}^{\text{TM},s})}{1 - R_{0+}^{\text{TM},s}R_{0-}^{\text{TM},s}} \frac{k_{\rho}^2}{8\pi\omega\epsilon_1} e^{ik_{1z}r_a} \right] \\ & H_1^{(1)'}[k_{\rho} | x_t - x_{t'} |] + \int_{-\infty}^{\infty} dk_{\rho} \frac{i\omega\mu_1}{k_{\rho}^2 |x_t - x_{t'}|} \left[i \frac{R_{0-}^{\text{TE},s}(1 + R_{0+}^{\text{TE},s})}{1 - R_{0+}^{\text{TE},s}R_{0-}^{\text{TE},s}} \frac{k_{\rho}^2}{8\pi k_{1z}} e^{-ik_{1z}r_a} + \right. \\ & \left. i \frac{(1 + R_{0+}^{\text{TE},s})}{1 - R_{0+}^{\text{TE},s}R_{0-}^{\text{TE},s}} \frac{k_{\rho}^2}{8\pi k_{1z}} e^{ik_{1z}r_a} \right] H_1^{(1)}[k_{\rho} | x_t - x_{t'} |], \\ E_{1x}^i(x_t) = & \int_{-\infty}^{+\infty} dk_{\rho} \frac{ik_{1z}}{k_{\rho}} (A_1 e^{ik_{1z}(h-r_a)} - B_1 e^{-ik_{1z}(h-r_a)}) H_1^{(1)'}(k_{\rho} | x_t |) + \\ & \int_{-\infty}^{+\infty} dk_{\rho} \frac{i\omega\mu_1}{k_{\rho}^2 |x_t|} (C_1 e^{ik_{1z}(h-r_a)} + D_1 e^{-ik_{1z}(h-r_a)}) H_1^{(1)}(k_{\rho} | x_t |). \end{aligned}$$

若可以求解出方程组(4)的解,便可得到系数 $P_{t'}$ 的值.

2.4 区域 0 中的散射场

在坐标系 (O_t, X_t, Z_t) 中,区域 1 中位于 $(x_{t'}, 0, h_1 + h_0)$ 的导体在入射场作用下产生的感应电流(偶极矩为 $P_{t'}$) 在介质 1 中的波幅 A_0^s, B_0^s, C_0^s 和 D_0^s 的值同样可以通过传播矩阵得到,此时偶极矩 $P_{t'}$ 在区域 0 中沿 x 方向的电场

$$\begin{aligned} E_{0x}^s = & \int_{-\infty}^{\infty} dk_{\rho} \frac{ik_{0z}}{k_{\rho}} (A_0^s(P_{t'})e^{ik_{0z}z'} - B_0^s(P_{t'})e^{-ik_{0z}z'}) H_1^{(1)'}(k_{\rho} | x' |) + \\ & \int_{-\infty}^{\infty} dk_{\rho} \frac{i\omega\mu_0}{k_{\rho}^2 |x'|} (C_0^s(P_{t'})e^{ik_{0z}z'} + D_0^s(P_{t'})e^{-ik_{0z}z'}) H_1^{(1)}(k_{\rho} | x' |), \\ E_{0z}^s = & \int_{-\infty}^{\infty} dk_{\rho} (A_0^s e^{ik_{0z}z'} + B_0^s e^{-ik_{0z}z'}) H_1^{(1)}(k_{\rho} | x' |). \end{aligned}$$

对空间固定坐标系 (K, ξ, ζ) 来说,墙体外散射场点 (x, y, z) 与坐标系 (O_t, X_t, Z_t) 的关系为: $x' = x - x_{t'}, y' = y, z' = z - h_1$. 此时在介质 1 中 m 段导体在 (x, y, z) 处产生的总的散射场

$$\begin{aligned} E_{0x}^s = & \int_{-\infty}^{\infty} dk_{\rho} \sum_{t'=1}^m \frac{ik_{0z}}{k_{\rho}} (A_0^s(P_{t'})e^{ik_{0z}(z-h_1)} - B_0^s(P_{t'})e^{-ik_{0z}(z-h_1)}) H_1^{(1)'}[k_{\rho} | x - x_{t'} |] + \\ & \int_{-\infty}^{\infty} dk_{\rho} \sum_{t'=1}^m \frac{i\omega\mu_0}{k_{\rho}^2 |x - x_{t'}|} (C_0^s(P_{t'})e^{ik_{0z}(z-h_1)} + D_0^s(P_{t'})e^{-ik_{0z}(z-h_1)}) H_1^{(1)}[k_{\rho} | x - x_{t'} |], \\ E_{0z}^s = & \int_{-\infty}^{\infty} dk_{\rho} \sum_{t'=1}^m (A_0^s(P_{t'})e^{ik_{0z}(z-h_1)} + B_0^s(P_{t'})e^{-ik_{0z}(z-h_1)}) H_1^{(1)}[k_{\rho} | x - x_{t'} |]. \end{aligned}$$

由推导可知,介质 1 中的散射场是与偶极矩 $P_{t'}$ 相关的,在得到方程组(4)的解后就可以计算出墙体外任一点的散射场.

3 理论计算与数值模拟比较

为了研究墙体中金属细导体目标的电磁散射问题,本文建立的物理模型如图 1 所示.一个细长金属导体

目标埋藏于厚度 $H=0.3$ m 的墙体中,偶极子天线的中心频率 $f=500$ MHz,墙体的相对介电常数 $\epsilon_1=0$,磁导率 μ_1 与自由空间磁导率 μ_0 相同。

图2虚线是采用本文方法计算出的介质1中距离墙体表面分别为0.7 m和1.0 m处的场强值 $|E_{0,x}^s|$ 随 x 变化的示意图,实线是采用时域有限差分数值模拟的结果,其中 $l=8.0$ m, $r_a=0.01$ m, $h_1=0.1$ m。从图2可知,1)场强 $|E_{0,x}^s|$ 是 x 的函数,沿着 x 方向有一个最大值,并且整个图形关于 $x=0$ 对称,这是因为计算过程中偶极子天线位于坐标轴中心,其散射场强度在 $x=0$ 最大;2)同一位置的偶极子源,当观测点与墙体之间的距离增大时,其散射场强度将会减小;3)相同场景下本文的计算方法与时域有限差分数值模拟结果符合良好。通过上述的分析计算以及与数值模拟的比较结果可知,本文提出的方法可以实现建筑物墙体中金属细导体目标散射场的计算和分析。

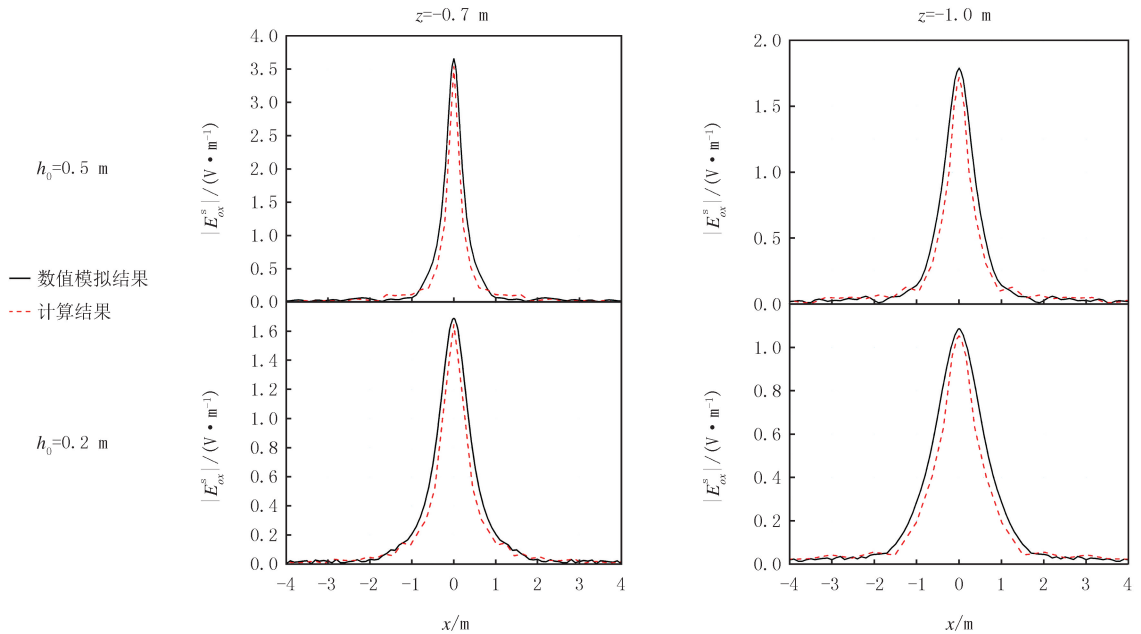


图2 2种方法下,散射场随 x 变化的示意图

Fig.2 Schematic diagram of the variation of scattering field with x under two methods

4 结论

本文针对实际工程应用中建筑物墙体结构探测雷达工作场景建立了物理模型,在此基础上利用分层介质中偶极子公式结合边界条件和矩量法提出了一种墙体中金属细导体目标的偶极子源计算方法,得到了墙体外任一点的散射场强度,最后将计算结果与数值模拟结果进行了比较,结果表明该方法能够实现对墙体中金属细导体目标散射场的计算和分析,可以为工程上建筑物墙体中目标的识别提供理论支持和参考依据。

参 考 文 献

- [1] LI J P, ZHANG L, QIN Q H. A regularized fast multipole method of moments for rapid calculation of three-dimensional time-harmonic electromagnetic scattering from complex targets[J]. *Engineering Analysis With Boundary Elements*, 2022, 142: 28-38.
- [2] AHMAD M. Fast method for solving integral equations of electromagnetic wave scattering from perfect conductor three-dimensional objects using Fourier series[J]. *Electromagnetics*, 2021, 41(6): 420-431.
- [3] CHEN Y L, JIANG X, LAI J, et al. A fast algorithm for the electromagnetic scattering from a large rectangular cavity in three dimensions [J]. *Journal of Computational Physics*, 2021, 437: 110331.
- [4] YU Y J, YU T J, CARIN L. Three-dimensional inverse scattering of a dielectric target embedded in a lossy half-space[J]. *IEEE Transactions on Geoscience and Remote Sensing*, 2004, 42(5): 957-973.
- [5] LIU Z J, HE J Q, XIE Y J, et al. Multilevel fast multipole algorithm for general targets on a half-space interface[J]. *IEEE Transactions on*

- Antennas and Propagation, 2002, 50(12):1838-1849.
- [6] PONTI C, SCETTINI G. The cylindrical wave approach for the electromagnetic scattering by targets behind a wall[J]. Electronics, 2019, 8(11):1262.
- [7] XU K W, ZHONG Y, CHEN X D, et al. A fast integral equation-based method for solving electromagnetic inverse scattering problems with inhomogeneous background[J]. IEEE Transactions on Antennas and Propagation, 2018, 66(8):4228-4239.
- [8] 詹华伟, 王良源, 陈思, 等. 基于 RSSI 的四边测距井下人员定位系统[J]. 河南师范大学学报(自然科学版), 2021, 49(4):53-59.
ZHAN H W, WANG L Y, CHEN S, et al. Four-sided ranging underground personnel positioning system based on RSSI[J]. Journal of Henan Normal University(Natural Science Edition), 2021, 49(4):53-59.
- [9] 赵燕峰, 娄海. 道路探地雷达在高速公路检测技术中的应用[J]. 河南师范大学学报(自然科学版), 2004, 32(2):98-100.
ZHAO Y F, LOU H. The applications and test technology with exploring land radar on expressway[J]. Journal of Henan Normal University(Natural Science Edition), 2004, 32(2):98-100.
- [10] 臧玉华, 陈静怡, 尚立, 等. 基于 TDOA 和 AOA 的 5G 室分场景三维定位方法[J]. 电力系统保护与控制, 2023, 51(2):180-187.
ZANG Y H, CHEN J Y, SHANG L, et al. Three-dimensional positioning method of a 5G indoor distribution system based on TDOA and AOA[J]. Power System Protection and Control, 2023, 51(2):180-187.
- [11] GAO J E, XIE Y J, YU H, et al. Characteristics of half-space electromagnetic scattering with multiple radiators[J]. AIP Advances, 2021, 11(4):045020.
- [12] 李雪萍, 纪奕才, 卢伟, 等. 车载探地雷达信号在分层介质中的散射特性[J]. 物理学报, 2014, 63(4):044201.
LI X P, JI Y C, LU W, et al. Characteristics of electromagnetic scattering from the vehicle-mounted ground penetrating radar in layered media[J]. Acta Physica Sinica, 2014, 63(4):044201.
- [13] ZU X B, BUTLER C M. Current induced by TE excitation on coupled and partially buried cylinders at the interface between two media[J]. IEEE Transactions on Antennas and Propagation, 1990, 38(11):1823-1828.
- [14] MARX E. Scattering by an arbitrary cylinder at a plane interface; broadside incidence[J]. IEEE Transactions on Antennas and Propagation, 1989, 37(5):619-628.
- [15] HU B, CHEW W C. Fast inhomogeneous plane wave algorithm for electromagnetic solutions in layered medium structures; two-dimensional case[J]. Radio Science, 2000, 35(1):31-43.
- [16] GUEUNING Q, DE LERA ACEDO E, BROWN A K, et al. An inhomogeneous plane-wave based single-level fast direct solver for the scattering analysis of extremely large antenna arrays[J]. IEEE Transactions on Antennas and Propagation, 2022, 70(10):9511-9523.
- [17] LIU S, ZOU B, ZHANG L M. An FDTD-based method for difference scattering from a target above a randomly rough surface[J]. IEEE Transactions on Antennas and Propagation, 2021, 69(4):2427-2432.
- [18] SUN L L, ZHAO F. Geometric attenuation factor based on scattering theory from randomly rough surface[J]. Applied Optics, 2021, 60(2):476-483.
- [19] TRIVEDI R, KHANKHOJE U K. A perturbative solution to plane wave scattering from a rough dielectric cylinder[J]. IEEE Transactions on Antennas and Propagation, 2015, 63(9):4069-4080.
- [20] 孔金欧. 电磁波理论[M]. 北京: 电子工业出版社, 2003.

Research on the characteristics of electromagnetic scattering from slim metal conductor buried in the wall

Li Xueping, Li Yuying, Zhang Qimeng, Li Wei

(College of Electronic and Electrical Engineering; Academician Workstation of Electromagnetic Wave Engineering of Henan Province, Henan Normal University, Xinxiang 453007, China)

Abstract: A physical model for the detection radar of the wall structure is established. Numerical computational method of electromagnetic scattering by slim metal conductor buried in the wall is proposed through the dipole method, and the scattering field is derived by boundary conditions combined with MOM. Then the results between the calculations and finite difference time domain method are compared. It shows that this method can calculate and analyze the electromagnetic scattering of the slim metal conductor buried in the wall quickly, and provide a fast algorithm to the detection radar imaging and electromagnetism inversion calculation.

Keywords: layered media; slim conductor; scattering property; dipole source